ARTICLE

Check for updates

Micro and nanoscale 3D printing using optical pickup unit from a gaming console

Tien-Jen Chang [1✉], Lukas Vaut[1], Martin Voss[1], Oleksii Ilchenko [1], Line Hagner Nielsen[1], Anja Boisen [1] & En-Te Hwu[1]

Conventional photopolymerization-based 3D printing still requires developing a concise and cost-effective method to improve the printing resolution at the nanoscale. Here, we propose the use of a gaming console optical drive pickup unit for 3D photopolymerization. This mass-produced optical pickup unit features a finely adjustable diode laser, allowing us to adjust the printing resolution from tens of micrometres down to hundreds of nanometres without requiring oxygen radical scavenging or costly femtosecond lasers. We evaluate the 3D printing performance using a commercial photopolymer under different laser exposure parameters. The proposed printing system achieves a resolution of 385 nm along the lateral direction and XYZ nano-resolution linear stages enable a printing volume of up to $50 \times 50 \times 25$ mm^3. Finally, we demonstrate the fabrication of 3D stereoscopic microstructures. The substantially simplified optics proposed here paves the way for affordable high-resolution micro/nanoscale 3D fabrication.

---

[1] The Danish National Research Foundation and Villum Foundation's Center for Intelligent Drug Delivery and Sensing Using Microcontainers and Nanomechanics (IDUN), Department of Health Technology, Technical University of Denmark, 2800 Kgs. Lyngby, Denmark. ✉email: tiech@dtu.dk

The 3D printing technology proposed in the 1980s has pioneered a new generation of manufacturing[1-3]. By the additive building of structures layer-by-layer, 3D printing allows the creation of stereoscopic structures that cannot be obtained using traditional subtractive manufacturing methods, such as cutting, milling, lathing and grinding[1,4]. Numerous ideas and materials have fostered the development of 3D printing techniques, including filament disposition modelling[5], selective laser sintering[6,7], PolyJet[8], aerosol jet printing[9], digital light processing[10,11], continuous liquid interface production[12,13], and stereolithography (STL)[14]. These manufacturing techniques have enabled the fabrication of innovative geometries to obtain structures with new properties and applications. For instance, unlike traditional methods, 3D printing can enhance location-specific material properties in aircraft turbines and bind multiple materials, thus constituting a novel application in aerospace manufacturing[15]. Moreover, personalised production has recently increased research on pharmaceutical applications regarding customised drug dosage systems for individual treatment, with 3D printing playing an important role in its development[16].

The resolution of a 3D printing system is described by the voxel size, which is the smallest 3D printed element that can be obtained while constructing a solid structure. Resolution varies according to the 3D printing technique. Macro 3D printers with millimetre-scale voxels are the most widely used and available on the market, whereas digital light processing and continuous liquid interface production provide voxel sizes down to tens of micrometres. Although it is difficult to obtain micro/nanoscale voxels, STL seems promising to achieve high-resolution 3D printing at such scales. STL applies a liquid photopolymer which mainly includes a photo-initiator, monomers, and oligomers. When the photopolymer is exposed to light at a specific wavelength, the photo-initiator absorbs the light energy and activates photopolymerization that cures the photopolymer into a solid structure[1]. The light energy distribution affects the cured voxel size[17-19], with voxel depth V_d being theoretically defined as

$$V_d = D_p \ln\left(\frac{E_0}{E_c}\right), \qquad (1)$$

where D_p is the penetration depth of the laser into the photopolymer, E_0 is the laser intensity on the photopolymer surface, and E_c is the critical exposure energy to start photopolymerization. In addition, voxel width V_w is defined as

$$V_w = W_0 \sqrt{2V_d/D_p}, \qquad (2)$$

where W_0 is the radius of the light beam. As W_0 is proportional to V_w, directing the light beam to a small focal spot during photopolymerization can substantially increase the 3D printing resolution.

Limited by the focal spot size, conventional STL systems reach a spatial resolution of 5 μm. Femtosecond laser-based 3D printers can print nanoscale structures, but the printing area is limited by the field of view of the objective lens (140 × 140 or 300 × 300 μm²). Moreover, the intricate stitching hinders printing at scales between micrometres and millimetres[20-22], and the complicated optics and expensive components prevent the widespread adoption of 3D printing based on femtosecond lasers.

There have been several attempts to achieve nanoscale photopolymerization in a cost effective fashion. A low-cost ultraviolet light emitting diode light source was proposed for a large area (over 1 × 1 cm²) nanoscale lithography system[23]. This system requires a two-stage optical setup that cannot construct multiple layer 3D structures. A less expensive quasi-continuous-wave 405-nm diode pulse laser (repetition rate: 1 MHz, duty cycle: 5–10%) is adopted to realise high-resolution 3D printing[24]. However, the

optical system is based on an expensive 3D printer (Photonics Professional GT, Nanoscribe, GmbH) and a Zeiss objective lens with a numerical aperture of 1.4. Both above mentioned systems share the common drawback that they require stitching process to achieve a millimetre or centimetre scale printing area.

The optical-pickup-unit (OPU) is a component for reading/writing data from optical storage discs such as Blu-rays, high-definition digital versatile discs (HD DVDs), DVDs, and compact discs (CDs)[25]. The mass produced OPU (costs less than five USD) provides not only a light source but also diffraction-limited optics in a compact size, similar to a car key. Given its high-precision measurements and multiple wavelength laser modes, the OPU has been used for various other applications, such as atomic force microscopy[26-28], biosensing[29,30], and photolithography[31]. The HD-DVD OPU equips an aspherical objective lens with a numerical aperture of 0.65, aperture diameter of 3 mm, and assumed laser beam quality of 1. Therefore, the OPU achieves a theoretical laser spot size of 430 nm in diameter ($1/e^2$ width) with the 405 nm laser, as indicated by Eq. (3)[25,32].

$$\text{Laser spot radius} = \frac{4\lambda f M^2}{\pi D}, \qquad (3)$$

where λ is the laser wavelength, f is the lens focal length, D is the input beam diameter at the lens, and M^2 is the laser beam quality. As the laser spot size is proportional to V_d in Eq. (2), the OPU laser spot delivers the required power for curing photopolymers at voxel sizes from tens of micrometres down to the nanoscale.

In this paper, we present the application of an OPU (Fig. 1a–c) as a compact and cost-effective solution to replace the conventional STL optical system and to eliminate the complexity of a STL system dramatically. An HD-DVD OPU extracted from a
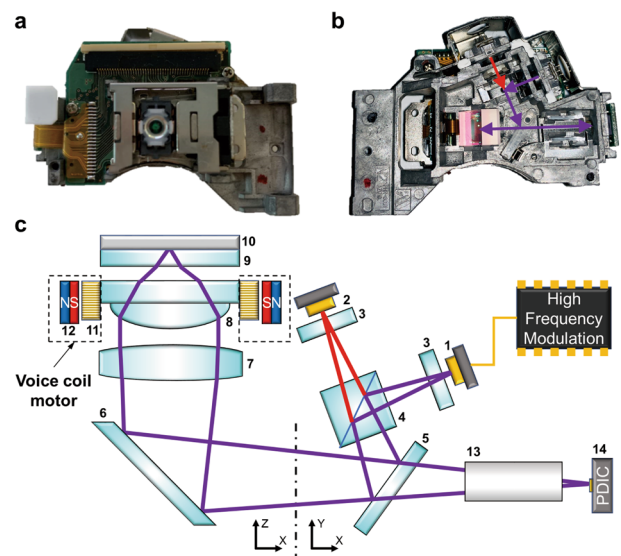

Fig. 1 High-definition digital versatile discs (HD DVDs) optical-pickup-unit (OPU) for 3D printing using photopolymerization. Photograph of HD DVDs OPU from **a** top view and **b** bottom view (the purple and red arrows indicate the optical path of 405 nm and 650/780 nm laser, respectively). **c** Intrinsic optical module, sensors, and actuators. 1: 405 nm laser diode, 2: 650/780 nm laser diode, 3: diffraction grating, 4: dichroic cube beam splitter, 5: beam splitter, 6: fold mirror, 7: collimating lens, 8: objective lens, 9: protective layer, 10: CD/DVD/HD-DVD disc data layer, 11: coil, 12: magnet, 13: expanding lens and 14: photodiode integrated circuit (PDIC). (The purple line represents 405 nm laser, while the red line represents 650/780 nm laser. Dot-dashed line indicates the transformation of view direction between *XY* panel and *XZ* panel.)

gaming console (Xbox 360; Microsoft, Redmond, WA, USA) has an optical working distance of 1.25 mm, which is four times that of a Blu-ray OPU, thus being more flexible for STL 3D printing. In addition, the HD-DVD OPU equips multiple-wavelength (405/650/780 nm) continuous wave semiconductor laser diodes to read HD-DVD/DVD/CD data, expanding the compatibility to various types and curing wavelengths of photopolymers. Although conventional multimaterial STL printing and multiple-step printing using different exposure wavelengths are under development[33–35], the OPU may substantially simplify the optical system design. The OPU also integrates an astigmatic optical path and a photodiode integrated circuit to generate the focus error signal (FES)[25], which is fed back for closed-loop laser focusing during the reading of data pits on a disc. A voice coil motor actuates the objective lens vertically and horizontally to compensate the disc wobbling and follow data tracks, respectively[25]. In the proposed OPU 3D printing system, the FES and voice coil motor are used for substrate parallelism correction (with non-photopolymer curing wavelength laser) and real-time fine-tuning of the printing level, respectively. This closed-loop printing mechanism further increases the performance of micro/nanoscale 3D printing compared to conventional open-loop STL systems. Finally, this 3D printing system realises multiple-layers 3D printed microstructure and achieves a nanoscale printing resolution along the lateral direction.

Results

OPU 3D printing system. Considering an inverted STL system[36], we designed a 3D printer with the laser spot directed upward. Figure 2a shows the developed OPU 3D printing system, which consists of XYZ linear stages, a tilt stage, a substrate holder, a photopolymer vat, an HD-DVD OPU, and a controlling system. The XY-axis linear stage positions the OPU for 2D printing, and the tilt stage mounted on the Z-axis stage adjusts the two-axis tilting angle of the substrate holder for optimal parallel positioning between the substrate and printing path. The OPU emits a 405 nm laser penetrating a transparent layer and focuses the laser inside the photopolymer vat (Fig. 2b, c). In the controlling system, an embedded controller connects to a customised OPU driver and a motor driver. The OPU driver adjusts the laser intensity, switches the laser wavelength, calculates the FES, and drives the voice coil motor. The motor driver controls the XY-axis and Z-axis linear stages with resolutions of 312.5 and 62.5 nm, respectively. The embedded controller communicates with a computer through a graphical user interface and implements the printing process via computer numerical control commands in G-code.

Conventional STL systems require external sensors for printing substrate levelling and achieving high-precision 3D printing. In contrast, the proposed OPU 3D printing system directly uses the embedded sensors to measure the distance between the focal spot and substrate surface at nanoscale resolution using the FES. The substrate surface and OPU focal plane can be precisely aligned in parallel by scanning the XY linear stage and adjusting the tilt stage (Fig. 2d). Levelling can also be performed with a non-curing laser wavelength (e.g., 650, 780 nm) when a 405 nm photopolymer is inside the vat. Before printing, the voice coil motor adjusts the objective lens along the Z direction for determining the photopolymer thickness. In addition, the FES determines whether the substrate surface reaches the focal spot (Fig. 2e). Thus, the OPU embedded sensing system can be used to optimise and increase the yield of micro/nanoscale 3D printing.

When levelling and calibration are complete, the G-code commands are executed for 3D printing, in which the Z-axis linear stage gradually lifts the substrate for realising layer-by-layer printing (Fig. 2f). The 3D structures are completed by washing out the residual resin with ethanol. For delicate and complex structures, the substrates are immersed in ethanol for 10 min for thorough washing.

Photopolymer thickness and laser spot size. The OPU provides an optimal focal spot on an HD-DVD track when the laser passes through air and a protective layer[25]. However, focusing the laser through the photopolymer distorts the focal condition given the higher refractive index (i.e., value defining the speed of light in a medium) of the photopolymer compared to air. According to the Snell's law, when the laser beam passes through the transparent layer into the next medium, its bending toward the normal line is higher in the photopolymer than in air. Consequently, laser divergence and an expanded focal spot with optical aberrations occur. To determine the optimal focus, we use the optical design software Zemax OpticStudio 20.1 (Zemax, Kirkland, WA, USA) to calculate the spot size at different photopolymer thicknesses, as this size represents the distance that the laser should travel through the photopolymer, as illustrated in Fig. 3a, b. This optical model is detailed in the optical path simulation section. As the objective lens concentrates the laser beam to pass through air and the protective layer, its simulated focal spot size is 454 nm ($1/e^2$ width). When the objective lens focuses the laser in a 25 μm thick photopolymer layer, the focal spot expands to 509 nm, and the maximum irradiance (energy per unit time) drops to 0.33. As the photopolymer layer thickness increases to 50, 75, and 100 μm, the focal spot further expands to 677, 720, and 816 nm, respectively, while the maximum irradiance drops to 0.18, 0.13, and 0.09, respectively. The simulation results show that increasing the photopolymer thickness reduces the laser energy concentration due to both the expanded focal spot size and reduced maximum irradiance.

Given the common focal spot divergence, a thick photopolymer layer reduces the printing resolution, as experimentally validated. The photopolymer thicknesses were set to 100, 75, 50, and 25 μm at fixed laser power of 2.40 μW. The system printed lines at speeds of 0.078–0.104 mm s^{-1} in a rectangular frame of 100×900 μm (width × length). The frame trapped the individual fragile line features. Figure 3c shows that the photopolymer thickness notably influences the printing performance, as the cured line width is smaller when decreasing the photopolymer thickness.

Laser exposure dose. In photopolymerization, the material dimension of the cured photopolymer exhibits a positive trend regarding laser exposure energy, as indicated by Eqs. (1) and (2). We controlled the laser exposure dose by adjusting both the printing speed and laser intensity to confirm this trend. For fixed laser power of 2.97 μW and photopolymer thickness of 25 μm, the developed system was used to print lines at different speeds from 0.104 to 0.138 mm s^{-1} in a rectangular frame of 100×900 μm (width × length), as shown in Fig. 4a. To determine the effect of laser intensity on the cured line width, this test was repeated at varying laser power of 2.64, 2.40, and 2.15 μW, obtaining the results shown in Fig. 4b–d, respectively. The trend of the cured width agreed with theory, as shown in Fig. 4e, as reducing the printing speed and increasing the laser intensity enhanced laser exposure, and thereby enlarging the cured line width.

Nanoscale printing resolution along the lateral direction. After system optimisation, we determined the highest achievable printing resolution by reducing the photopolymer thickness. Using the FES closed-loop feedback, the voice coil motor can precisely focus the laser spot on the silicon substrate. Figure 5a
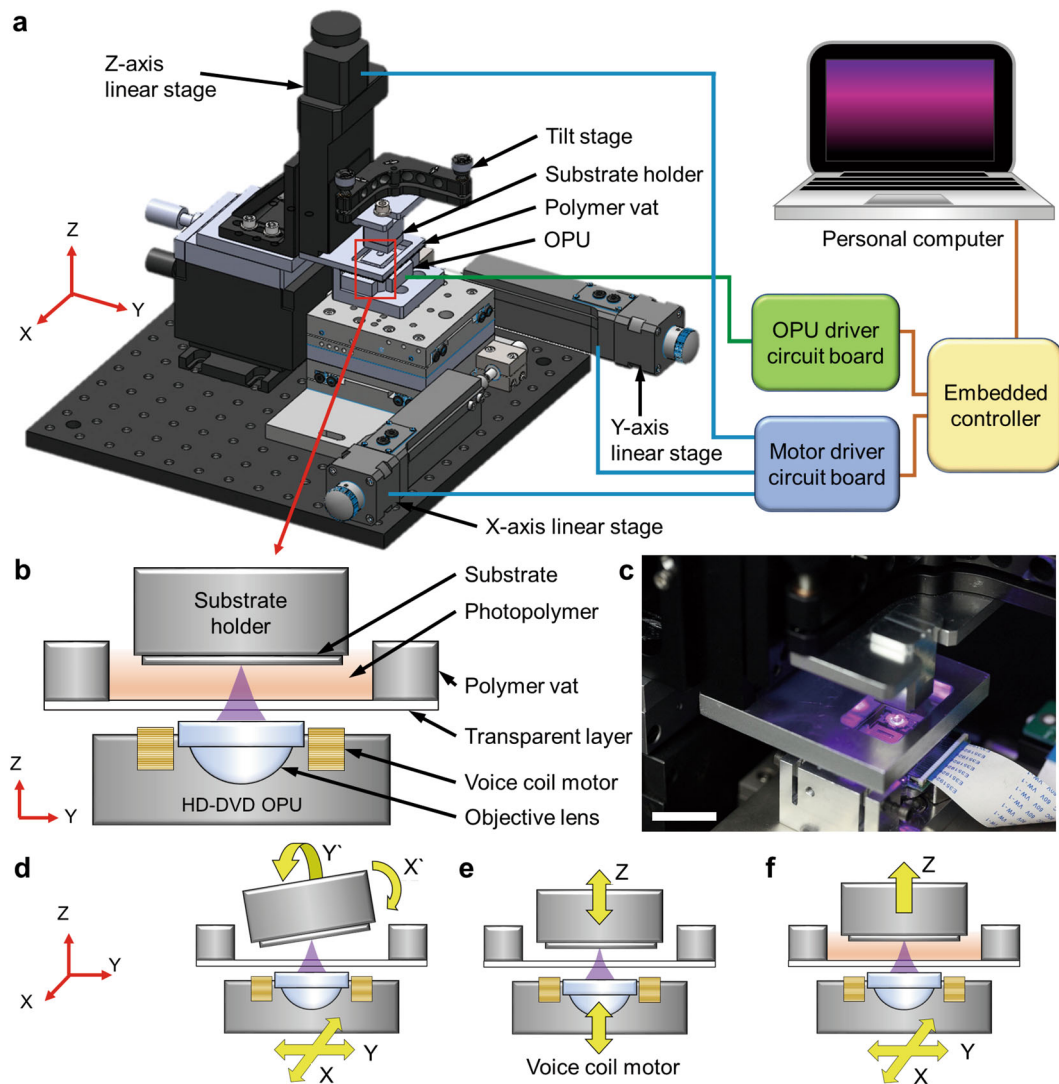
Fig. 2 Developed 3D printer using high-definition digital versatile discs (HD DVDs) optical-pickup-unit (OPU) as core optical module by focusing laser beam of 405 nm wavelength to cure photopolymer in Vat. a Mechanism of printer with inverted stereolithography (STL) design and control system diagram. **b** Detailed diagram of optical path. **c** Photograph of system during printing (scale bar represents 2 cm). **d** Substrate tilting diagram (X' and Y' represent tilting substrate along X-axis and Y-axis, respectively). **e** Vertical position initialisation and objective lens translation diagrams. **f** Printing solid structures layer-by-layer process diagram. These diagrams are illustrative and do not reflect the real scales.

shows a $300 \times 300\,\mu m$ square printed with lines with a width of approximately $3\,\mu m$ using a photopolymer of $13\,\mu m$ in thickness. After further reducing the photopolymer thickness to $6\,\mu m$, we achieved nanoscale linear structures along the lateral direction at different printing speeds with fixed laser power of $2.40\,\mu W$, as shown in Fig. 5b–e. The nanostructures were suspended by two vertical structures with a $15\,\mu m$ separation. The width of the nanostructures decreased to 992, 879, 769, and 385 nm with increasing printing speeds of 0.16, 0.18, 0.21, and $0.25\,mm\,s^{-1}$, respectively. A cross-section contour of a 385 nm wide line shows the laser energy distribution in Fig. 5f. Figure 5g shows the line width according to the printing speed, as the nanostructures can be printed repeatedly using the same parameter settings. To the best of our knowledge, this is the first system to print nanoscale structures along the lateral direction using a low-cost OPU with a continuous wave diode laser source.

3D printed structures. To verify the performance of the proposed OPU 3D printing system, we fabricated various 3D microstructures, as shown in Fig. 6. Figure 6a shows an 850-μm-

high pyramid printed with layers of 25 μm in height. Figure 6b, c show a tilted square tower and a twisted tower, respectively. These 3D microstructures were printed without stitching. Furthermore, the cylinder being 300 μm in diameter and 150 μm in height shown in Fig. 6d was printed to demonstrate printing following curved paths. Figure 6e shows a structure resembling a gate with around 800 μm in length and 400 μm in height, demonstrating the ability to print structures with overhanging features.

Discussion
Printer design and substrate adhesion. The design of the proposed OPU 3D printer can improve substrate alignment and printing layer control. Instead of moving the photopolymer vat along the horizontal direction, the *XY* linear stage directly drives the OPU, mitigating unstable liquid vibration by acceleration-induced and deceleration-induced forces. This printer has a maximum printing volume of $50 \times 50 \times 25\,mm^3$ that can be unlimitedly enlarged by replacing the mechanical components such as with a wider substrate, larger polymer vat, and longer
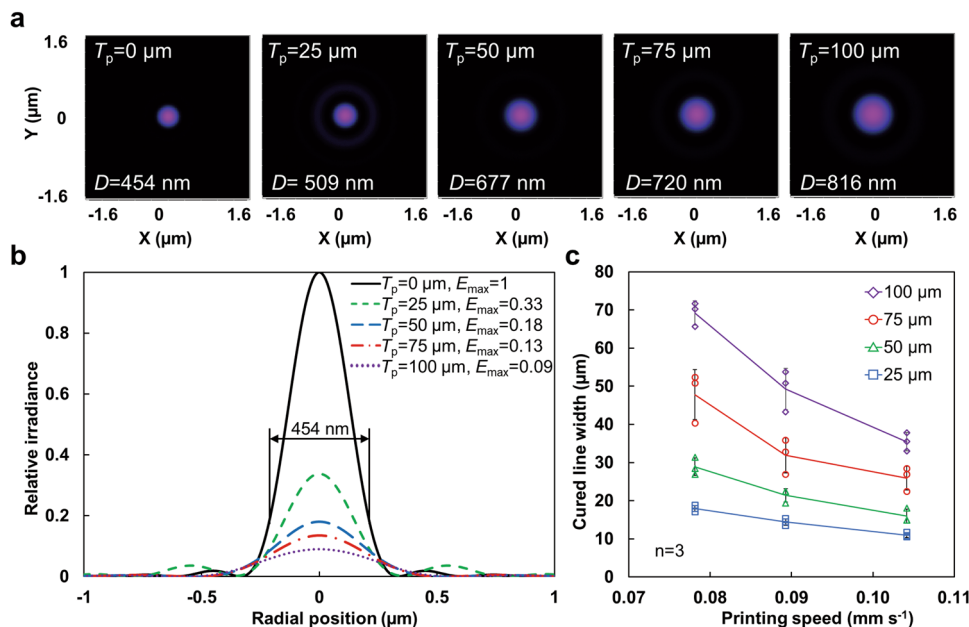
Fig. 3 Effect of photopolymer thickness on cured line width obtained from optical simulation software and experimentally validated. a Laser focal spot simulated in Zemax OpticStudio 20.1 at photopolymer thicknesses, T_p, of 0, 25, 50, 75, and 100 μm, with spot diameters, D, of 454, 509, 677, 720, and 816 nm, respectively. **b** Laser focal spot energy Gaussian distribution and maximum irradiance, E_{max}, at various photopolymer thicknesses. **c** Printing results illustrating the relation between the cured line width and printing speed at various photopolymer thicknesses (n represents sample size, while error bars represent one standard deviation).
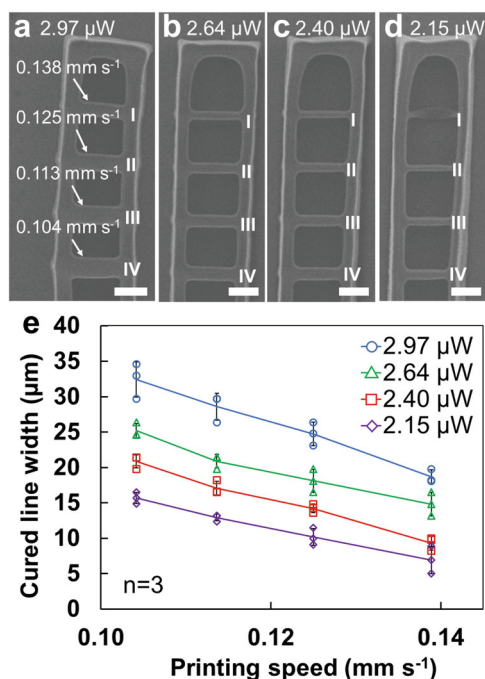

Fig. 4 Laser exposure dose verification by printing straight lines in a rectangular frame structure at varying printing speed and laser intensity. Scanning electron microscope images of cured lines at laser powers of **a** 2.97, **b** 2.64, **c** 2.40, and **d** 2.15 μW (scale bar represents 50 μm). The printing speed was set to 0.104, 0.113, 0.125, and 0.138 mm s^{-1} corresponding to labels I, II, III, and IV, respectively. **e** Cured line width according to printing speed at various laser intensities (n represents sample size, while error bars represent one standard deviation).
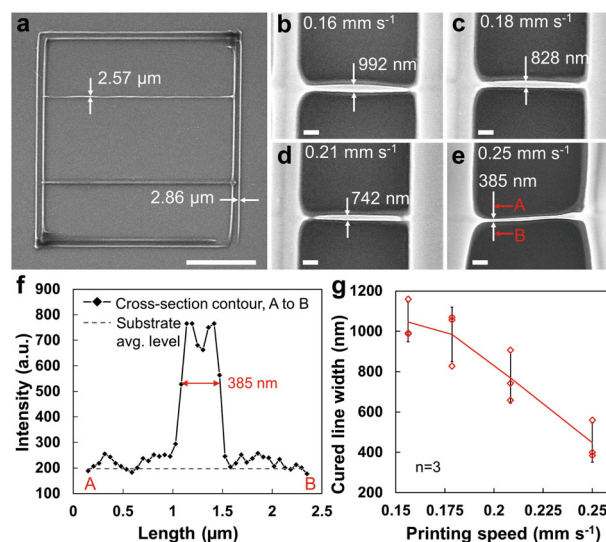

Fig. 5 Scanning electron microscope images of 3D printed nanoscale structures. a 300 × 300 μm square printed with microscale lines with a width of approximately 3 μm (scale bar represents 100 μm). The nanoscale structures were cured at printing speeds of **b** 0.16, **c** 0.18, **d** 0.21, and **e** 0.25 mm s^{-1}, resulting in line widths of 992, 879, 769, and 385 nm, respectively. Two vertical lines (width approximately 5 μm) were printed with a distance of 15 μm to suspend the nanometre structures (scale bars represent 2 μm). **f** Cross-section contour of 385-nm-width structure in **e**. **g** Cured nanoscale width according to printing speed at a laser power of 2.40 μW and a photopolymer thickness of 6 μm (n represents sample size, while error bars represent one standard deviation).
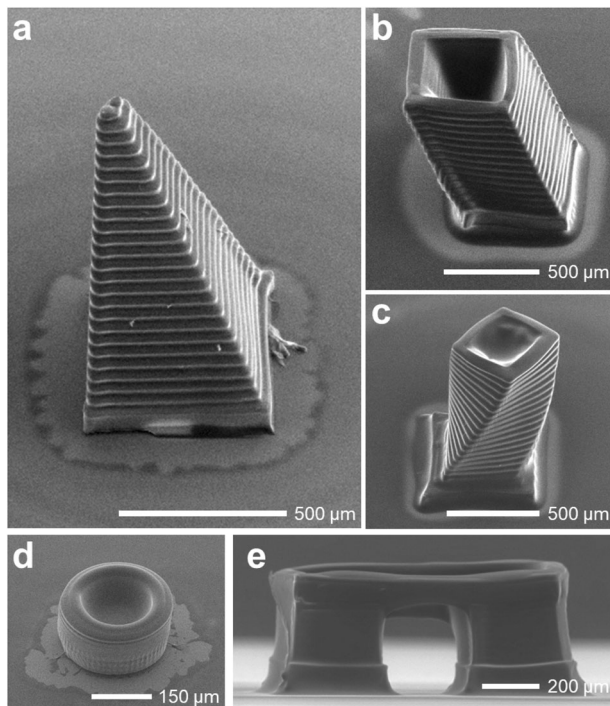
Fig. 6 Scanning electron microscope images of 3D printed structures. a Pyramid with height of approximately 850 μm and height of 25 μm per layer. **b** Tilted square tower. **c** Twisted tower. **d** Cylinder. **e** Gate-like structure.

working distance linear stages. Still, a potential drawback of our method is the possible curing of all the photopolymer between the substrate and the transparent layer, causing the printed structure to adhere to the transparent layer. Typically, continuous liquid interface production relies on oxygen inhibition to prevent the cured photopolymer from adhering to the transparent layer by applying an oxygen-penetrable film[12]. For maintaining optical path completeness, we used a polymethyl methacrylate (PMMA) film to support the photopolymer and a silicon substrate to carry the cured material. Compared to PMMA, the silicon surface has higher surface energy, providing more stable adhesion of the printed structures. In addition, we printed a thicker foundation layer with higher laser exposure to support the cured structures on the substrate. The 3D structures shown in Fig. 6 show this substrate adhesion method for strong support.

Laser exposure control boundary. We were able to predict the critical exposure energy for curing the photopolymer during tests of laser intensity and printing speed through an exposure dose evaluation at laser power of 2.40 μW and printing speed of 0.104 mm s^{-1}. Although the highest laser power from the OPU is 0.2 mW, we used lower power in this study. Hence, the printing speed may be increased by applying higher laser intensity to balance the laser exposure. However, reaching the theoretical maximum speed of the stages is constrained by various factors. To raise the positioning resolution, we used a one-sixteenth step to drive the stage, thus reducing the linear speed. In addition, high current for increasing the driving motor speed caused a sudden temperature rise in the motor, changing the photopolymer temperature and destabilising the printing environment. Moreover, vibration constrained the maximum feasible speed for 3D printing, as a high speed matching the system resonant frequency caused oscillation. The printer vibration was monitored along the Z-axis using the FES. To increase the printing speed,

high-resolution linear positioning stages (e.g., piezo-driving stage, linear motor stage) should be adopted, enabling low vibration, and temperature consistency.

Photopolymer thickness and nanoscale structures. From the optical simulation, we confirmed that reducing the photopolymer thickness led to a smaller and more concentrated focal spot. Moreover, an analysis of the experimental results using multiple regression showed that the coefficient of photopolymer thickness is the most significant factor determining the cured line width. Thus, reducing the photopolymer thickness can lead to increased resolution. However, the depth of the focal laser spot and printer mechanical structure limit the minimum thickness of the printed photopolymer. Currently, the thinnest tested layer of the photopolymer is 6 μm. The cross-section contour characterised by scanning electron microscopy in Fig. 5f reflects the OPU laser energy distribution. The printer cures nanoscale linear structures with a width of 385 nm, which is below the laser spot size of 430 nm, and close to theatrical limitation of 311 nm, calculated by Fraunhofer diffraction formula of a grating[37]. Unlike a Gaussian distribution with a single peak, the contour shows two peaks, which might reflect the optical module's laser energy distribution. The central point is approximately 18% below the two peaks. The main reason for this phenomenon might be an optical aberration. Thus, the 6 μm thick photopolymer layer setting still causes optical aberration that limits the maximum irradiance point and leads to the splitting into two peaks[38].

Through precisely controlling laser exposure dosage and photopolymer thickness, the printer can reach printing nanoscale structures along the lateral direction. However, the system presents some printing uncertainty, as shown in Fig. 5a, f. The high-resolution printing is sensitive to photopolymer thickness variation which locally changes the laser energy distribution. As the PMMA transparent layer (Fig. 2b) has a relatively large suspension area (30 × 60 mm^2), an inconsistent photopolymer thickness may easily arise due to geometry deviations such as layer flatness, surface scratches, plastic deformation, and parallel misalignment to the substrate.

Polygonal structures. In 3D printing, STL is the most common file format for describing 3D structures given its efficiency and universality to transfer various kinds of structures. The STL format cuts a structure into numerous triangular facets. Then, a computer transforms the STL file into G-code commands, which are used by the printer to move along the straight lines of the triangle edges for depicting the patterns at each layer. Although, the STL format has many benefits, it compromises the smoothness of curved surfaces. In Fig. 6d, we divided the cylinder perimeter into sixty line segments for the printer to generate the rounded shape, resulting in surface discontinuity. We speculate that a curve function might prevent this problem. In G-code, clockwise and counter-clockwise curve functions (G02 and G03, respectively) can be adopted to control a two-axis motor and execute round motions to obtain smooth continuous surfaces.

Enlarged corners. By closely examining the printed structure in Fig. 6a, we observe that the corner structure is slightly larger (~120%) than the other printed features. This is due to the motor slowing down and then speeding up when printing corners. Consequently, the laser has a relatively longer exposure time in that area, causing the larger rounded features shown in the figure. This phenomenon can be eliminated by compensating the laser intensity near corners to obtain uniform structures. In addition, the large rounded corners are caused by the photopolymer

accumulating more energy when two laser exposure points are close[10], being another aspect that remains to be addressed.

Conclusion

We successfully constructed a nanometre resolution 3D printer relying on an off-the-shelf OPU to cure a photopolymer. The printer successfully produces microscale 3D structures layer-by-layer, and the OPU allows to achieve nanoscale printing resolution of 385 nm along the lateral direction, outperforming any commercially available STL printer. By leveraging the OPU operation and built-in electronics, the developed 3D printing system presents many benefits regarding aspects such as reduced cost, compactness, closed-loop control, and unconstrained printing area. Therefore, the proposed OPU 3D printer can be a high-performance alternative for photopolymerization-based 3D printing. Furthermore, the compact nature of the OPU enables the possibility of using 2×2 or 3×3 OPU arrays to parallelise 3D printing for multiplying throughput. As the proposed printer can print millimetre or micrometre scale devices with nanoscale lateral resolution, it has great potential for mass-producing or scaling up the fabrication of microdevices with intricate designs, such as microscale vessels for drug delivery, microactuators, microscale medical devices, and micro-optical components.

Methods

Developed 3D printer components and mechanism. The core optical component of the gaming console HD-DVD drive OPU was the PRH-803T model (Toshiba, Tokyo, Japan) that integrates a laser diode modulation integrated circuit (ATR0885; Atmel, San Jose, CA, USA). The tilt stage (KM200V; Thorlabs, Newton, NJ, USA) was used to align the substrates with ±4° of precision tilt adjustment. The vertical linear stage (LM60-25; OWIS, Staufen, Germany) was used to move the substrate along the Z axis with 25 mm travel distance. The two-axis horizontal positioning linear stage (LNR50S, Thorlabs), including the platform and linear stepper motor, has a travel distance of 50 mm along each direction. To drive the three linear stages, we used a motor driver (A4988; Allegro MicroSystems, Manchester, NH, USA) supporting at most 16 divisions per step. The controller (myRIO-1900; National Instruments, Austin, TX, USA) was operated at clock frequency of 667 MHz considering its digital and analogue inputs/outputs for control. The software was developed by the authors, and the system programme was implemented on the LabVIEW 2016 software (National Instruments). The main structure of the printer was made of aluminium. The substrate, photopolymer vat, and OPU holder were manufactured using a milling process via computer numerical control.

Material preparation for 3D printing. We selected a commercially available white photopolymer (FLPGWH02; Formlabs, Somerville, MA, USA) as printing material with curing process activated by 405 nm wavelength light, which corresponds to the operation wavelength of the HD-DVD OPU reading laser. The solvent for washing the residual photopolymer after printing was 95% ethanol. To prepare the silicon surface for carrying the cured structure, a chemical mechanical polishing silicon wafer was sliced into a 12×12 mm^2 square by a grinding saw machine. The silicon surface flatness was below 1 μm. The PMMA layer for loading the photopolymer was a clear plate with thickness of 0.5 mm. A CO_2 laser was used to cut the PMMA into a 30×60 mm^2 rectangle. The PMMA refractive index was 1.5051 when 405-nm wavelength light penetrated the polymer.

Measurement of laser power and dimension of cured solid structure. To characterise the laser strength, a laser power metre (PM100D; Thorlabs) was used to measure the laser intensity directly from the objective lens. After printing, a tabletop scanning electron microscope (TM3030 Plus; Hitachi, Tokyo, Japan) was used to characterise the microscale structures. A 45° tilted sample holder carried the specimen for accurate and detailed spatial feature observation.

Optical path simulation. We used Zemax OpticStudio 20.1 to simulate the laser divergence as the objective lens focused the laser beam into the photopolymer. Given that the OPU geometry parameter of the objective lens was not provided by the manufacturer, we first tried to obtain the geometry structure by optimising an aspherical objective lens which concentrated a 405 nm wavelength parallel laser beam to pass through 0.75 mm thick air layer and focused on a 0.5 mm thick PMMA layer. The objective lens was simulated with glass BK7 of 1.7 mm in thickness. The backside geometry parameters included radius of 6.913 mm, clear semi-diameter of 1.5 mm, mechanical semi-diameter of 1.5 mm, 2nd-order term of 0.317, 4th-order term of 0.019, 6th-order term of $-2.663E-03$, 8th-order term of $-8.701E-04$, and 10th-order term of $-1.421E-03$. The facade geometry

parameters included radius of 5.16 mm, clear semi-diameter of 1.288 mm, mechanical semi-diameter of 1.5 mm, 2nd-order term of -0.054, 4th-order term of 0.011, 6th-order term of $-6.168E-03$, 8th-order term of $-5.320E-04$, and 10th-order term of $-2.466E-04$. After obtaining the objective lens with diffraction-limited performance, its position was shifted toward the PMMA layer to simulate focusing the laser inside the photopolymer layer (refractive index of 1.50). When the laser travelled through the photopolymer layer, the laser focal spot expanded, and the focal distance increased. By shifting the objective lens 25, 50, 75 and 100 μm toward the PMMA layer, we obtained distances (inside the photopolymer) between the PMMA and focal spot of 41, 78, 117 and 155 μm, respectively. In addition, the simulated focal laser spot diameters, D, inside the photopolymer were 509, 677, 720 and 816 nm, as shown in Fig. 3a, b, and the maximum irradiance values were 0.33, 0.18, 0.13 and 0.09, respectively.

Reporting summary. Further information on research design is available in the Nature Research Reporting Summary linked to this article.

Data availability

The data that support the findings of this study are available from the corresponding author on reasonable request.

Code availability

All code and software generated during this study are available from the corresponding author on request.

References

1. Ligon, S. C., Liska, R., Stampfl, J., Gurr, M. & Mülhaupt, R. Polymers for 3D printing and customized additive manufacturing. *Chem. Rev.* **117**, 10212–10290 (2017).
2. Kodama, H. Automatic method for fabricating a three-dimensional plastic model with photo-hardening polymer. *Rev. Sci. Instrum.* **52**, 1770–1773 (1981).
3. Bártolo, P. J. & Gibson, I. in *Stereolithography: Materials, Processes and Applications* (ed. Bártolo, P. J.) Ch. 2 (Springer, 2011).
4. Vaezi, M., Seitz, H. & Yang, S. A review on 3D micro-additive manufacturing technologies. *Int. J. Adv. Manuf. Technol.* **67**, 1721–1754 (2013).
5. Mohamed, O. A., Masood, S. H. & Bhowmik, J. L. Optimization of fused deposition modeling process parameters: a review of current research and future prospects. *Adv. Manuf.* **3**, 42–53 (2015).
6. Tan, K. H. et al. Scaffold development using selective laser sintering of polyetheretherketone–hydroxyapatite biocomposite blends. *Biomaterials* **24**, 3115–3123 (2003).
7. Gibson, I. & Shi, D. Material properties and fabrication parameters in selective laser sintering process. *Rapid Prototyp. J.* **3**, 129–136 (1997).
8. Gaynor, A. T., Meisel, N. A., Williams, C. B. & Guest, J. K. Multiple-material topology optimization of compliant mechanisms created via PolyJet three-dimensional printing. *J. Manuf. Sci. Eng.* **136**, 061015 (2014).
9. Hoey, J. M., Lutfurakhmanov, A., Schulz, D. L. & Akhatov, I. S. A review on aerosol-based direct-write and its applications for microelectronics. *J. Nanotechnol.* **2012**, 1–22 (2012).
10. Sun, C., Fang, N., Wu, D. M. & Zhang, X. Projection micro-stereolithography using digital micro-mirror dynamic mask. *Sens. Actuators A Phys.* **121**, 113–120 (2005).
11. Kowsari, K. et al. Photopolymer formulation to minimize feature size, surface roughness, and stair-stepping in digital light processing-based three-dimensional printing. *Addit. Manuf.* **24**, 627–638 (2018).
12. Tumbleston, J. R. et al. Continuous liquid interface production of 3D objects. *Science* **347**, 1349–1352 (2015).
13. Janusziewicz, R., Tumbleston, J. R., Quintanilla, A. L., Mecham, S. J. & DeSimone, J. M. Layerless fabrication with continuous liquid interface production. *Proc. Natl Acad. Sci.* **113**, 11703–11708 (2016).
14. Maruo, S. & Ikuta, K. Submicron stereolithography for the production of freely movable mechanisms by using single-photon polymerization. *Sens. Actuators A Phys.* **100**, 70–76 (2002).
15. Misra, A. K., Grady, J. E. & Carter, R. Additive manufacturing of aerospace propulsion components. 1–21 http://ntrs.nasa.gov/archive/nasa/casi.ntrs.nasa.gov/20150023067.pdf (2015).
16. Goole, J. & Amighi, K. 3D printing in pharmaceutics: a new tool for designing customized drug delivery systems. *Int. J. Pharm.* **499**, 376–394 (2016).

17. Jacobs, P. F. In *Rapid Prototyping & Manufacturing: Fundamentals of Stereolithography* (ed. Reid, D. T.) Ch. 3–4 (Society of Manufacturing Engineers, 1992).

18. Lee, J. H., Prud'Homme, R. K. & Aksay, I. A. Cure depth in photopolymerization: experiments and theory. *J. Mater. Res.* **16**, 3536–3544 (2001).

19. Zhang, X., Jiang, X. N. & Sun, C. Micro-stereolithography of polymeric and ceramic microstructures. *Sens. Actuators A Phys.* **77**, 149–156 (1999).

20. Reiner, R. R., Tanguy, Y. & Hoffmann, J. Process for producing a three-dimensional structure (2016).

21. Maruo, S., Nakamura, O. & Kawata, S. Three-dimensional microfabrication with two-photon-absorbed photopolymerization. *Opt. Lett.* **22**, 132–134 (1997).

22. Xiong, W., Jiang, L. J., Baldacchini, T. & Lu, Y. F. In *Laser Additive Manufacturing: Materials, Design, Technologies, and Applications* (ed. Brandt, M.) Ch. 9 (Elsevier, 2017).

23. Wen, S. B., Bhaskar, A. & Zhang, H. Scanning digital lithography providing high speed large area patterning with diffraction limited sub-micron resolution. *J. Micromech. Microeng.* **28**, 075011 (2018).

24. Mueller, P., Thiel, M. & Wegener, M. 3D direct laser writing using a 405 nm diode laser. *Opt. Lett.* **39**, 6847–6850 (2014).

25. Hwu, E. T. & Boisen, A. Hacking CD/DVD/Blu-ray for biosensing. *ACS Sens.* **3**, 1222–1232 (2018).

26. Hwu, E. T., Illers, H., Jusko, L. & Danzebrink, H. U. A hybrid scanning probe microscope (SPM) module based on a DVD optical head. *Meas. Sci. Technol.* **20**, 084005 (2009).

27. Hwu, E. T. et al. Anti-drift and auto-alignment mechanism for an astigmatic atomic force microscope system based on a digital versatile disk optical head. *Rev. Sci. Instrum.* **83**, 013703 (2012).

28. Liao, H. S. et al. Operation of astigmatic-detection atomic force microscopy in liquid environments. *Rev. Sci. Instrum.* **84**, 103709 (2013).

29. Segerink, L. I., Koster, M. J., Sprenkels, A. J. & van den Berg, A. A low-cost 2D fluorescence detection system for μm sized beads on-chip. *Lab Chip* **12**, 1780–1783 (2012).

30. Barathur, R. et al. New disc-based technologies for diagnostic and research applications. *Psychiatr. Genet.* **12**, 193–206 (2002).

31. Rothenbach, C. A. & Gupta, M. C. High resolution, low cost laser lithography using a Blu-ray optical head assembly. *Opt. Lasers Eng.* **50**, 900–904 (2012).

32. Blu-ray Disc Association. White Paper Blu-Ray Disc™ Format. 1–48 http://www.blu-raydisc.com/Assets/Downloadablefile/White_Paper_General_4th_20150817_clean.pdf (2010).

33. Choi, J. W., Kim, H. C. & Wicker, R. Multi-material stereolithography. *J. Mater. Process. Technol.* **211**, 318–328 (2011).

34. Han, D., Yang, C., Fang, N. X. & Lee, H. Rapid multi-material 3D printing with projection micro-stereolithography using dynamic fluidic control. *Addit. Manuf.* **27**, 606–615 (2019).

35. Zhang, X., Xi, W., Huang, S., Long, K. & Bowman, C. N. Wavelength-selective sequential polymer network formation controlled with a two-color responsive initiation system. *Macromolecules* **50**, 5652–5660 (2017).

36. Taormina, G., Sciancalepore, C., Messori, M. & Bondioli, F. 3D printing processes for photocurable polymeric materials: technologies, materials, and future trends. *J. Appl. Biomater. Funct. Mater.* **16**, 151–160 (2018).

37. Fischer, J. & Wegener, M. Three-dimensional optical laser lithography beyond the diffraction limit. *Laser Photonics* **7**, 22–44 (2013).

38. Alkelly, A. A. Spot size and radial intensity distribution of focused Gaussianbeams in spherical and non-spherical aberration lenses. *Opt. Commun.* **277**, 397–405 (2007).

Acknowledgements

Author contributions

T.J.C. and L.V. designed and built the mechanism and electronic control system of the 3D printer. T.J.C developed the LabVIEW programme for the 3D printer. T.J.C. and M. V. optimised the printing parameters and conducted the printing process. E.T.H initiated the OPU 3D printing concept and provided technical consultancy for implementing the HD-DVD pickup unit. T.J.C and O.I. built the optical model and simulated the optimisation. E.T.H., L.H.N., and A.B. supervised the experiments. T.J.C., E.T.H., and L.H.N. wrote the manuscript with the assistance of all authors.

Competing interests

The authors declare no competing interests.

Additional information

Supplementary information The online version contains supplementary material available at https://doi.org/10.1038/s42005-021-00532-4.

Correspondence and requests for materials should be addressed to T.-J.C.

Reprints and permission information is available at http://www.nature.com/reprints

Publisher's note Springer Nature remains neutral with regard to jurisdictional claims in published maps and institutional affiliations.